ORGANOMETALLICS

Article

pubs.acs.org/Organometallics

Hydride Reduction of NAD(P)$^+$ Model Compounds with a Ru(II)−Hydrido Complex

Kichitaro Koga,[†] Yasuo Matsubara,[‡] Tatsumi Kosaka,[§] Kazuhide Koike,[∥] Tatsuki Morimoto,[⊥] and Osamu Ishitani*[,†]

[†]Department of Chemistry, Graduate School of Science and Engineering, Tokyo Institute of Technology, O-okayama 2-12-1-NE-1, Meguro-ku, Tokyo 152-8550, Japan

[‡]Department of Material and Life Chemistry, Kanagawa University, Rokkakubashi 3-27-1, Kanagawa-ku, Yokohama 221-8686, Japan

[§]Graduate School of Science and Engineering, Saitama University, 255 Shimo-Okubo, Saitama 338-8570, Japan

[∥]National Institute of Advanced Industrial Science and Technology, Onogawa 16-1, Tsukuba 305-8569, Japan

[⊥]Department of Applied Chemistry, School of Engineering, Tokyo University of Technology, 1401-1 Katakura, Hachioji, Tokyo 192-0982, Japan

Supporting Information

ABSTRACT: In order to better understand the regioselective hydride transfer of metal hydrido complexes to NAD(P)$^+$ model compounds, reactions of [Ru(tpy)(bpy)H]$^+$ (**Ru-H**: tpy = 2,2′:6″,2″-terpyridine, bpy = 2,2′-bipyridine) with various substituent NAD(P)$^+$ model compounds were investigated in detail. All of the NAD(P)$^+$ model compounds accepted hydride from **Ru-H**, yielding 1:1 adducts, where the dihydro form(s) of the model compounds coordinated with the carbamoyl group to the Ru(II) center of [Ru(tpy)(bpy)]$^{2+}$, with very different reaction rates. Some reactions produced the adduct with only the 1,4-dihydro structure, whereas others produced a mixture of two adducts, with a 1,4- or 1,2-dihydro structure. In particular, temperature-dependent adduct formation kinetics studies provided important information on the transition state(s) of the hydride transfer reactions and factors for determining the regioselectivity. Most adducts were cleaved to the corresponding free dihydro product(s) with the same distribution of the regioisomers to the adduct(s).

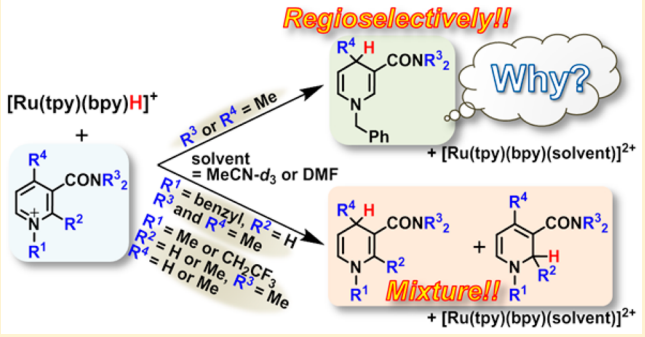

INTRODUCTION

In various biological redox reactions, the coenzyme NAD(P)$^+$ serves as an oxidant and accepts a hydride from various substrates, including water and ethanol. This process selectively yields the 1,4-dihydro product NAD(P)H in the presence of enzymes, including the Fd-NADP$^+$ reductase[1] and alcohol dehydrogenase.[2] Alternatively, in artificial reduction systems without the enzymes, the corresponding NAD(P)$^+$ model compounds are reduced by hydride donors such as $NaBH_4$, to not only the 1,4-dihydro form but also its structural isomers, i.e., 1,2- and 1,6-dihydro products (eq 1).[3]

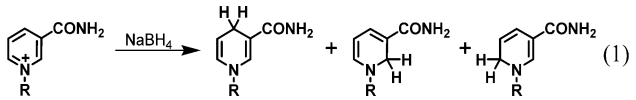

(1)

It is known that NAD(P)$^+$ model compounds can be regioselectively reduced to the corresponding 1,4-dihydro form via metal hydrido complexes.[4,5] For example, [Rh(Cp*)(bpy)(H_2O)]$^{2+}$[5c,d] and [Ir(Cp*)(L)(H_2O)]$^{2+}$[4b,c] (Cp* = 1,2,3,4,5-pentamethylcyclopentadiene, bpy = 2,2′-bipyridine, L = 4-(1*H*-pyrazol-1-yl-κN^2)-benzoate-κC^3) can serve as catalysts along with formate or H_2 as reductants, selectively producing the corresponding 1,4-NAD(P)H models. In these catalytic reactions, the metal hydrido complexes were presumed to be intermediates, which provided a hydride to the NAD(P)$^+$ model compound.[5c,d] Although the production selectivity of the 1,4-dihydro form during the hydride-transfer process is assumed to result from the interaction between the carbamoyl group at the C-3 position of the NAD(P)$^+$ model compound and the metal center in the transition state,[5d,6] direct evidence and detailed properties of the intermediates have not been reported to date. We have reported on the photocatalytic and regioselective hydride reduction of a typical NAD(P)$^+$ model compound, 1-benzyl-3-carbamoylpyridinium cation (**1a**), using [Ru(tpy)(bpy)(NEt_3)]$^{2+}$ (tpy = 2,2′:6″,2″-terpyridine) as a photocatalyst and NEt_3 as a reductant.[6,7] In the beginning of the reaction, [Ru(tpy)(bpy)H]$^+$ is formed via the photoexcitation of [Ru(tpy)(bpy)(NEt_3)]$^{2+}$ (process 1 in Scheme 1).[7c,d]

Received: August 18, 2015

DOI: 10.1021/acs.organomet.5b00713
Organometallics XXXX, XXX, XXX−XXX

Scheme 1. Reaction Mechanism of the Photocatalytic Reduction of 1a using $[Ru(tpy)(bpy)(NEt_3)]^{2+}$ as a Photocatalyst and NEt_3 as a Reductant[6,7]

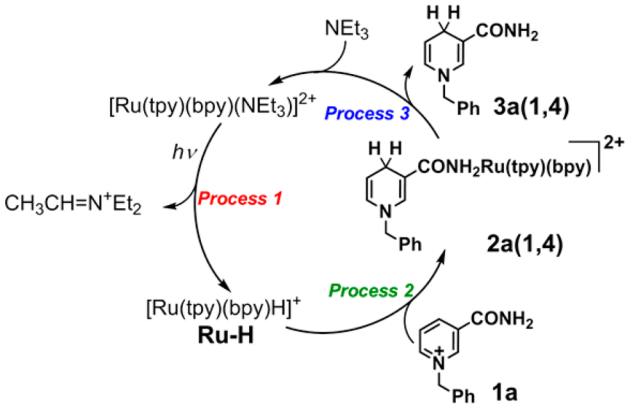

The product **Ru-H** rapidly reacts with **1a** to give the corresponding 1,4-dihydro product. The reaction between the hydrido complex **Ru-H** and **1a** was investigated in detail.[6,7d] In the initial reaction step, the 1:1 adduct **2a(1,4)** producing the 1,4-dihydro form **3a(1,4)** coordinated with its carbamoyl group to the Ru(II) center of $[Ru(tpy)(bpy)]^{2+}$ (process 2). **2a(1,4)** quantitatively cleaved at a much slower rate, yielding free **3a(1,4)**. $[Ru(tpy)(bpy)(NEt_3)]^{2+}$ was recovered at the same time (process 3).

The observation that the carbamoyl group coordinated with the metal center in the intermediate **2a(1,4)** is the first clear evidence that the interaction between the carbamoyl group and the metal center plays an important role in the hydride transfer reaction transition state, particularly for inducing the regioselective formation of the 1,4-dihydro product.[7b] Because a "seven-coordinated" Ru(II) complex was produced in the transition state, where the carbamoyl group of **1a** interacts with Ru(II) and the hydride ligand interacts with the C-4 position of the pyridinium unit, the hydride could not transfer to the C-6 position, which is farther from the carbamoyl group in comparison with the C-4 position. However, it is unclear why the hydride did not transfer to the C-2 position of the pyridinium unit of **1a**, which is located approximately at the same distance from the carbamoyl group as the C-4 position. The addition of steric and/or electronic perturbations to the NAD(P)$^+$ model compound could help in clarifying this. However, the reactions of NAD(P)$^+$ model compounds with substituent groups at the C-2 and/or C-4 positions with **Ru-H** have not been reported.

Many asymmetric reduction systems of various carbonyl compounds using chiral NAD(P)H model compounds with a methyl group at the C-4 position as a reductant have been reported.[8] For example, the NAD(P)$^+$ model compounds shown in eqs 2[8a] and 3[8e] could transfer the hydride to the substrates in high optical yields.

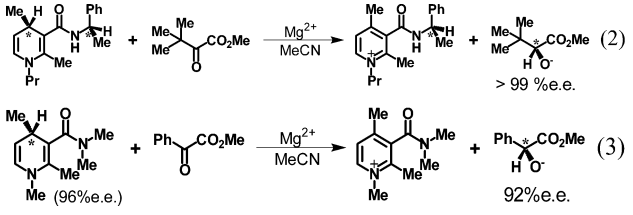

However, these reactions require an equimolecular amount of the NAD(P)H model compounds in comparison with the unsaturated substrate. To use the NAD(P)H model compounds as catalysts, new systems that can recover the NAD(P)H model compounds with the same chirality by hydride reduction of the oxidized model compounds are required. Although the metal hydrido complexes are candidates as the reductant because they can (photo)catalytically supply a hydride for the NAD(P)$^+$ model compounds, as described above, reactions of the metal hydrido complexes with the NAD(P)$^+$ model compounds that exhibit a substituent at the C-4 position and various substituents at the N-1 and/or C-3 positions have not been reported.

We herein report reactions of **Ru-H** with various NAD(P)$^+$ model compounds comprising a methyl group at the C-4 position and/or substituents at other position(s) to understand their steric and electronic effects on the regioselectivity and rate of hydride transfer (Chart 1).

Chart 1. Structures of NAD(P)$^+$ Model Compounds

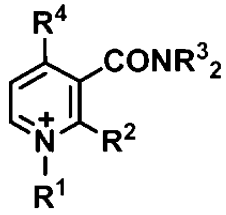

	R^1	R^2	R^3	R^4
1a	Benzyl	H	H	H
1b	Benzyl	H	H	Me
1c	Benzyl	H	Me	H
1d	Benzyl	H	Me	Me
1e	Me	H	Me	H
1f	CH_2CF_3	H	Me	H
1g	CH_2CF_3	H	Me	Me
1h	CH_2CF_3	Me	Me	Me

RESULTS

Product Analyses. As an example, in a typical reaction, **Ru-H** (8.0 mM) and **1b** (8.4 mM) were mixed in MeCN-d_3 and monitored using ^{1}H NMR (Figure 1). The signals of **Ru-H**

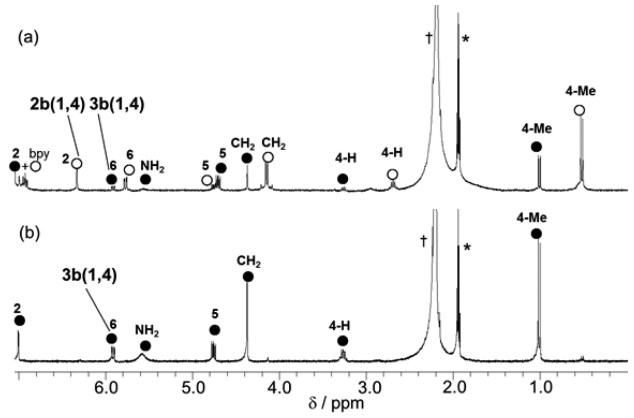

Figure 1. ^{1}H NMR spectra of an MeCN-d_3 solution containing **Ru-H** (8.0 mM) and **1b** (8.4 mM), which were kept at room temperature in the dark for (a) 20 min and (b) 20 h. The peaks marked with ○, ●, †, and * are attributed to **2b(1,4)**, **3b(1,4)**, water, and the solvent, respectively.

completely disappeared 20 min after mixing. Alternatively, the 1:1 adduct **2b(1,4)**, where **1b** was selectively reduced to the corresponding 1,4-dihydro product **3b(1,4)** and coordinated

DOI: 10.1021/acs.organomet.5b00713
Organometallics XXXX, XXX, XXX−XXX

with the Ru(II) center with the carbamoyl group at the C-3 position of the dihydropyridine moiety, free **3b(1,4)** and the solvent complex $[Ru(tpy)(bpy)(MeCN\text{-}d_3)]^{2+}$ were also detected as minor products, which should form via cleavage of the 1:1 adduct **2b(1,4)** (eq 4). The reaction solution was held at

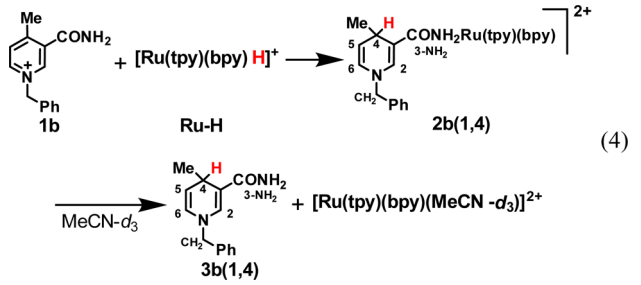

(4)

room temperature for 20 h, resulting in the cleavage of **2b(1,4)** to give **3b(1,4)** and $[Ru(tpy)(bpy)(MeCN\text{-}d_3)]^{2+}$ in a quantitative yield. Hence, the respective 1,2- and 1,6-dihydro isomers of **2b(1,4)** and **3b(1,4)** were not detected at all.

Conversely, when **1d** (8.4 mM) was used instead of **1b** in a similar experiment, 1:1 adducts exhibiting both the 1,4-dihydropyridine moiety **2d(1,4)** and 1,2-dihydropyridine moiety **2d(1,2)** were produced (eq 5 and Figure 2). A reaction time

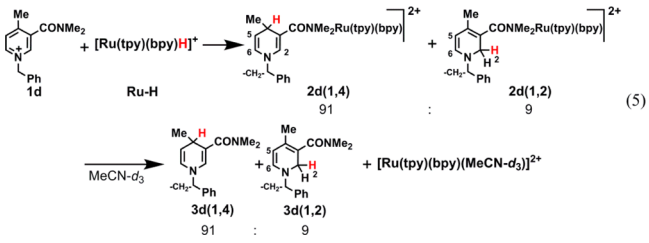

(5)

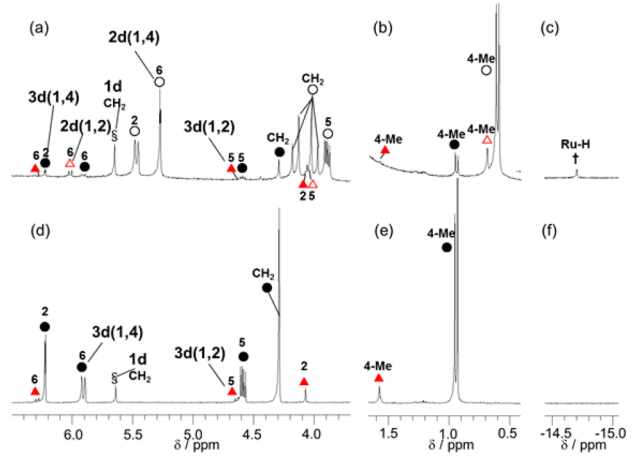

Figure 2. ^{1}H NMR spectral changes in an MeCN-d_3 solution containing **Ru-H** (8.0 mM) and **1d** (8.4 mM) at room temperature after 25 min (a–c) and 20 h (d–f) (red △, **2d(1,2)**; black ○, **2d(1,4)**; red ▲, **3d(1,2)**; black ●, **3d(1,4)**). The peaks marked with § and † were attributed to CH_2 at the benzyl group of **1d** and the hydrido ligand of **Ru-H**, respectively.

of 6 h was required to completely remove the signals for **1d** and **Ru-H** when the product ratios did not change from the initial state to the end: i.e., [**2d(1,4)**]:[**2d(1,2)**] = 91:9. The reaction mixture was kept at room temperature for 1 day, resulting in the cleavage of both 1:1 adducts, yielding $[Ru(tpy)(bpy)(MeCN\text{-}d_3)]^{2+}$ and the corresponding free dihydropyridines, with a ratio of 91:9 between **3d(1,4)** and **3d(1,2)**, respectively.[9]

Similar experiments were conducted using different $NAD(P)^+$ model compounds. The results are summarized in Table 1. All of the $NAD(P)^+$ model compounds, which were only converted to the 1:1 adduct with the 1,4-dihydropyridine moiety, had a benzyl group at the N-1 position of the pyridinium moiety (**1a–c**). The only exception was **1d**, which had a benzyl group at the N-1 position and methyl groups both at the C-4 position and at the N atom of the carbamoyl group; this product was converted to a 1:1 adduct with either a 1,4- or a 1,2-dihydropyridine moiety (**2g(1,4)**, **2g(1,2)**) with a 91:9 ratio. In the $NAD(P)^+$ models with a methyl group (**1e**) or a 2,2,2-trifluoroethyl group (**1f–h**), the mixtures of the two 1:1 adducts, with a 1,4- or 1,2-dihydropyridine moiety, were produced in different ratios. In the cleavage reaction of the 1:1 adduct(s), isomerization of the dihydropyridine moiety was not observed, except for the reaction of **1g** and **Ru-H**. The ratio of **2g(1,4)** to **2g(1,2)** was 29:71 immediately after mixing **1g** and **Ru-H**. However, the ratio of **3g(1,4)** to **3g(1,2)** was 43:57 after the cleavage reaction was completed.

Kinetic Analysis of the Reactions of Ru–H with the $NAD(P)^+$ Model Compounds. The reactions of **Ru-H** with the $NAD(P)^+$ model compounds were followed with the stopped-flow method. As an example, Figure 3 shows the change in the UV–vis absorption spectra of a DMF solution containing **Ru-H** (0.031 mM) mixed with another DMF solution containing an excess amount of **1b** (3.8 mM) at 300 K. During the first 200 s after mixing (Figure 3a), a set of isosbestic points was observed at 419 and 502 nm, with a decrease in the absorption band at λ_{max} 535 nm attributed to **Ru-H** and an increase in another absorption band at λ_{max} 490 nm. As described above, ^{1}H NMR of the reaction solution clearly indicated that these changes in the absorption spectra were attributable to the formation of the 1:1 adduct **2b(1,4)**. Figure 3b shows the spectral changes for longer reaction times, up to 24 h; the absorption band at λ_{max} 490 nm shifted to larger wavelengths, and its intensity increased. These changes are attributed to the cleavage of **2b(1,4)** to **3b(1,4)** and $[Ru(tpy)(bpy)(DMF)]^{2+}$.

Figure 4 shows the change in the absorbance at 535 nm, which enables analysis of the **2b(1,4)** reaction rate of formation. This decay curve can be fitted with pseudo-first-order kinetics (eq 6; the derivation is shown in Supporting Information, and the same experiments were repeated six times for each temperature). The pseudo-first-order reaction rate constant (k_{obs}) was determined as $(1.18 \pm 0.01) \times 10^{-2}$ s^{-1}. Using eq S2 in the Supporting Information and the values $k_{obs} = (1.18 \pm 0.01) \times 10^{-2}$ s^{-1} and the initial concentration of **1b** $[\mathbf{1b}]_{int} = 1.9$ mM, the second-order reaction rate constant of formation of **2b(1,4)** was calculated as $k = 6.20 \pm 0.06$ M^{-1} s^{-1}.[11]

$$A = (\varepsilon_{\mathbf{Ru\text{-}H}} - \varepsilon_{\mathbf{2b(1,4)}})[\mathbf{Ru\text{-}H}]_{int} e^{-k_{obs}t} + \varepsilon_{\mathbf{2b(1,4)}}[\mathbf{Ru\text{-}H}]_{int} \quad (6)$$

where A, ε, t, and $[\mathbf{Ru\text{-}H}]_{int}$ are the absorbance at 535 nm, the molar extinction constant, the reaction time after mixing, and the initial concentration of **Ru-H**, respectively.

Similar measurements at different reaction temperatures in the range 280–320 K gave linear Eyring plots, as shown in Figure 5: $y = -(4.29 \pm 0.06)x + (10.4 \pm 0.2)$. The activation parameters, $\Delta H^{\ddagger}$ and $\Delta S^{\ddagger}$, were found to be 35.7 ± 0.4 kJ mol^{-1} and -111 ± 1 J mol^{-1} K^{-1}, respectively. Similar experiments were conducted using the other $NAD(P)^+$ model compounds (Figures S8 and S10–S14 in the Supporting Information), except for **1d**, because the formation rate of the adducts was

DOI: 10.1021/acs.organomet.5b00713
Organometallics XXXX, XXX, XXX–XXX

Table 1. Ratios of the Product Structural Isomers, Second-Order Rate Constants, and Activation Parameters of the Reactions of Ru−H with the $NAD(P)^+$ Model Compounds

	position				1,4:1,2						
	1	2	3[a]	4	2	3	k[b], M^{-1} s^{-1}	$\Delta G^{\ddagger}$[b], kJ mol^{-1}	$\Delta H^{\ddagger}$, kJ mol^{-1}	$-T\Delta S^{\ddagger}$[b], kJ mol^{-1}	$\Delta S^{\ddagger}$, J mol^{-1} K^{-1}
1a	benzyl	H	H	H	100:0	100:0	(2.92 ± 0.04) × 10^3	53.6 ± 0.3	23.9 ± 0.3	29.6 ± 0.3	(−9.88 ± 0.09) × 10
1b	benzyl	H	H	Me	100:0	100:0	6.20 ± 0.06	68.9 ± 0.6	35.7 ± 0.4	33.2 ± 0.4	(−1.11 ± 0.01) × 10^2
1c	benzyl	H	Me	H	100:0	100:0	(6.09 ± 0.04) × 10^2	57.5 ± 0.2	25.5 ± 0.2	32.0 ± 0.2	(−1.07 ± 0.01) × 10^2
1d	benzyl	H	Me	Me	91:9	91:9					
(1,4)[c]							1.8 × 10^{-1}	78 ± 2	57 ± 1	20 ± 1	(−6.8 ± 0.4) × 10
(1,2)[d]							1.9 × 10^{-2}	83 ± 3	61 ± 2	22 ± 2	(−7.5 ± 0.6) × 10
1e	Me	H	Me	H	96:4	96:4	(7.49 ± 0.02) × 10	62.7 ± 0.3	34.0 ± 0.2	28.7 ± 0.2	(−9.57 ± 0.07) × 10
1f	CH_2CF_3	H	Me	H	73:27	73:27	(1.29 ± 0.06) × 10^4	49.9 ± 0.2	23.9 ± 0.2	25.9 ± 0.2	(−8.64 ± 0.06) × 10
1g	CH_2CF_3	H	Me	Me	29:71	43:57	(5.94 ± 0.01) × 10	63.3 ± 0.2	31.2 ± 0.1	32.1 ± 0.1	(−1.07 ± 0.00) × 10^2
1h	CH_2CF_3	Me	Me	Me	96:4	96:4	7.66 ± 0.04	68.3 ± 0.3	36.8 ± 0.2	31.6 ± 0.2	(−1.05 ± 0.01) × 10^2

[a]Two methyl groups were introduced into the nitrogen atoms of the carbamoyl group at the C-3 position. [b]At 300 K. [c]Formation of **2d(1,4)**. [d]Formation of **2d(1,2)**.

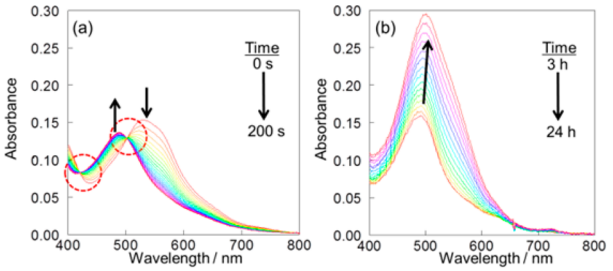

Figure 3. Changes in UV−vis spectra after mixing a DMF solution containing **Ru-H** (0.031 mM) and a DMF solution containing **1d** (3.8 mM) at 300 K (a) for 0−200 s and (b) for 3−24 h.

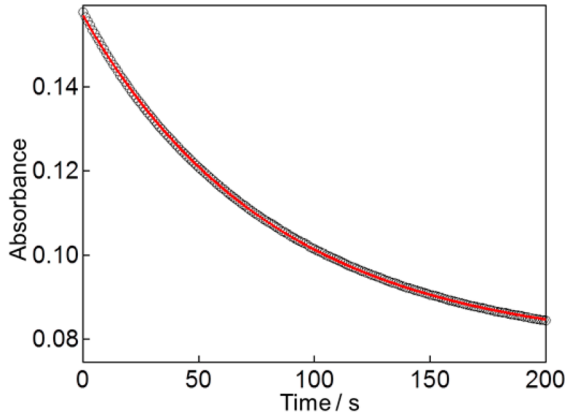

Figure 4. Decay of the absorbance measured at 535 nm after a DMF solution containing **Ru-H** (0.031 mM) and a DMF solution containing **1b** (3.8 mM) were mixed at 300 K (○). The red solid curve is the result of fitting with eq 6 ($y = 0.0793 \times e^{-0.0120t} + 0.0777$).

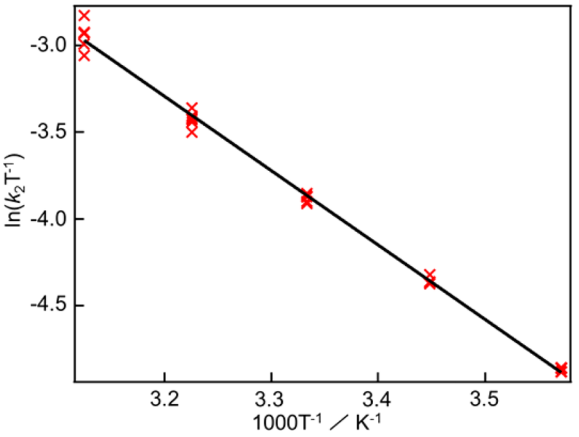

Figure 5. Eyring plots for the formation of **2b** in DMF measured at 280−320 K. The same measurements were repeated 6 times.

too slow to be measured with the stopped-flow method. The derived k values and the activation parameters are summarized in Table 1.

In the case of **1d**, the adduct formation reaction was much slower, while the rate of solvolysis was not much changed: this leads to competing kinetics that could be monitored on the NMR time scale. This gave us a chance to follow the formation processes of each adduct, **2d(1,2)** or **2d(1,4)**, separately using ^{1}H NMR. Figure 6 shows time-dependent changes in the substrates, adducts, and final products when reacting **Ru-H** (8.0 mM) with an equal amount of **1d** in DMF-d_7 at 300 K. They can be reasonably modeled with a global fitting method on the basis of

DOI: 10.1021/acs.organomet.5b00713
Organometallics XXXX, XXX, XXX−XXX

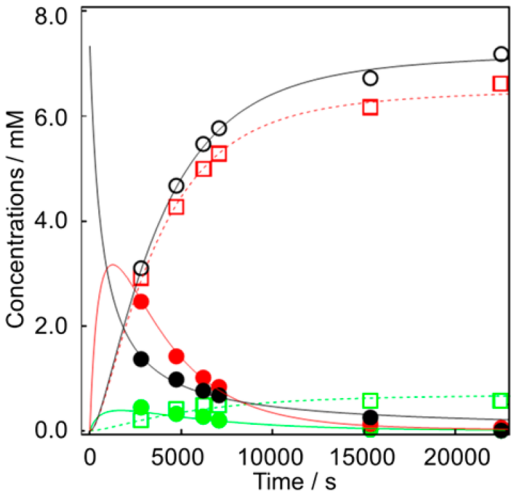

Figure 6. Time dependencies of **Ru-H** (black ●), **2d(1,2)** (green ●), **2d(1,4)** (red ●), **3d(1,2)** (green □), and **3d(1,4)** (red □) concentrations in the reaction of **Ru-H** (8.0 mM) and **1d** (8.0 mM) in DMF-d_7 at 300 K. The fitting curves using eqs 7−11 are also shown.

Scheme 2. Reaction of Ru-H with 1d in DMF-d_7

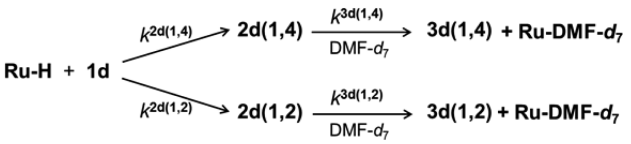

eqs 7−11 (Scheme 2), which gave the adduct formation rates for **2d(1,2)** and **2d(1,4)** as $k^{2d(1,2)}$ = 1.9 × 10^{-2} M^{-1} s^{-1} and $k^{2d(1,4)}$ = 1.8 × 10^{-1} M^{-1} s^{-1}, respectively.

$$\frac{d[\mathbf{Ru\text{-}H}]}{dt} = -(k^{2d(1,4)} + k^{2d(1,2)})[\mathbf{Ru\text{-}H}][\mathbf{1d}] \quad (7)$$

$$\frac{d[\mathbf{2d(1,4)}]}{dt} = k^{2d(1,4)}[\mathbf{Ru\text{-}H}][\mathbf{1d}] - k^{3d(1,4)}[\mathbf{2d(1,4)}] \quad (8)$$

$$\frac{d[\mathbf{2d(1,2)}]}{dt} = k^{2d(1,2)}[\mathbf{Ru\text{-}H}][\mathbf{1d}] - k^{3d(1,2)}[\mathbf{2d(1,2)}] \quad (9)$$

$$\frac{d[\mathbf{3d(1,4)}]}{dt} = k^{3d(1,4)}[\mathbf{2d(1,4)}] \quad (10)$$

$$\frac{d[\mathbf{3d(1,2)}]}{dt} = k^{3d(1,2)}[\mathbf{2d(1,2)}] \quad (11)$$

Eyring plots of **2d(1,2)** and **2d(1,4)** formation showed good linearity at 300−320 K (Figure S15 in the Supporting Information), which was independently used to derive the activation parameters for both adducts (Table 1).

DISCUSSION

The reaction of **Ru-H** with **1b**,**c**, which have methyl group(s) either at the C-4 position or on the N atom of the carbamoyl group at the C-3 position, gave only the adduct with the 1,4-dihydropyridine structure, without the formation of its positional isomers: i.e., the corresponding adducts with the 1,2- or 1,6-dihydro structure (Table 1 and eq 4). These reaction rates were slower than the reaction rate of **Ru-H** with **1a**, although the product distribution was the same. In the case of **1b**, particularly with the methyl group at the C-4 position, the reaction rate was much slower than that in the case of **1a** by 1/470 at 300 K. In the case of **1c**, the reaction rate was reduced by 1/5 in comparison to that in the case of **1a**. It has been proposed that the reaction of **Ru-H** with **1a** proceeds via the transition state with a seven-coordinated six-membered-ring structure, where the carbamoyl group interacts with the Ru center and the hydride ligand interacts with the carbon atom at the C-4 position (Scheme 3).[10,7b,11] For **2b(1,4)** formation, $\Delta H^{\ddagger}$ was

Scheme 3. Schematic Structures in the Transition State in the Reaction of Ru−H with 1a[a]

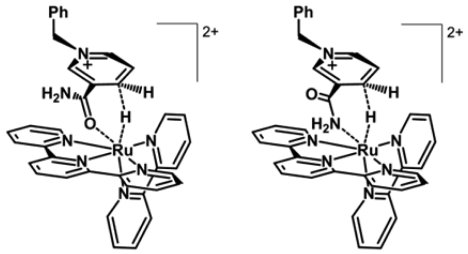

[a]The difference in the structures is the coordination atom of **1a** to the Ru center: oxygen in **I(a-1)** and nitrogen in **I(a-2)**.[10]

much larger than that for **2a(1,4)**, by 11.8 ± 0.5 kJ mol^{-1} (Table 1), mainly because of the electron-donating property of the methyl group, which should be the major reason the reaction between **1b** and **Ru-H** was much slower. In contrast, the difference in the entropic term was relatively lower ($\Delta(-T\Delta S^{\ddagger})_{2b(1,4)\text{-}2a(1,4)}$ = 3.6 ± 0.5 kJ mol^{-1} at 300 K). On the other hand, for **2c(1,4)** formation, the increase in $\Delta H^{\ddagger}$ ($\Delta\Delta H^{\ddagger}_{2c(1,4)\text{-}2a(1,4)}$ = 1.6 ± 0.4 kJ mol^{-1}) was significantly less than that for **2b(1,4)** formation ($\Delta\Delta H^{\ddagger}_{2b(1,4)\text{-}2a(1,4)}$ = 11.8 ± 0.5 kJ mol^{-1}), whereas the increase in $-T\Delta S^{\ddagger}$ at 300 K from the formation of **2a(1,4)** was similar to that in the case of **1b** ($-T\Delta S^{\ddagger}$ = 29.6 ± 0.3 kJ mol^{-1} for the formation of **2a(1,4)**; 33.2 ± 0.4 kJ mol^{-1} for **2b(1,4)**; 32.0 ± 0.2 kJ mol^{-1} for **2c(1,4)**). The introduction of the methyl groups into the carbamoyl group at the C-3 position should induce both an increase in the nucleophilicity of the amide group and a decrease in the positive charge of the carbon atom at the C-4 position of the pyridinium ring. The former should be advantageous for transition state formation in the reaction of **Ru-H** with **1c**, whereas the latter should be disadvantageous. The introduction of the methyl group(s) into the carbamoyl group or into the C-4 position caused an increase in $-T\Delta S^{\ddagger}$ (Table 1). This is likely due to steric restrictions of the methyl group(s) on the seven-coordinated transition-state structure (Scheme 3).

We already clarified that the N atom of the carbamoyl group coordinates the central ruthenium ion in the *oxidized* adduct which was constructed with the deprotonated **1a** and $[Ru(tpy)(bpy)]^{2+}$ using spectroscopic and X-ray crystallographic analyses; on the other hand, the O atom of the *deprotonated* carbamoyl group coordinates the central ruthenium ion in the reduced adduct which was constructed with the *deprotonated* **3a(1,4)** and $[Ru(tpy)(bpy)]^{2+}$, i.e., *deprotonated* **2a(1,4)**.[6] Unfortunately, the X-ray crystallographic data of **2a(1,4)** itself have not been obtained because of its instability and spectroscopic data of **2a(1,4)** could not give clear evidence for determining the coordinating atom to the Ru(II) center.[7b] Using the DFT method, therefore, we calculated the stabilities of "**2a(1,4)**"

DOI: 10.1021/acs.organomet.5b00713
Organometallics XXXX, XXX, XXX−XXX

and "**2c(1,4)**" with a Ru−O or Ru−N bond as typical examples with a carbamoyl group or a dimethyl carbamoyl group (Figure S16 in the Supporting Information); this indicated that the O atom is clearly more favorable for coordination to the Ru center than that with the N atom in the case of **2c(1,4)** with the dimethyl carbamoyl group because of steric hindrance of the methyl groups on the N atom ($\Delta\Delta G_{(Ru-N)-(Ru-O)}$ = 74.1 kJ mol^{-1}). In the case of **2a(1,4)** with the carbamoyl group, on the other hand, the N coordination was thermodynamically more stable even though the difference between the two coordination modes was much smaller ($\Delta\Delta G_{(Ru-N)-(Ru-O)}$ = −9.66 kJ mol^{-1}). These results suggest that the coordination mode between the Ru center and the NAD(P)H model in **2**, and possibly in the transition state, might change depending on the structure of the carbamoyl group.

In the case of **1d** with the methyl groups in both the C-4 position and the carbamoyl group, the main product was still the 1,4-dihydro adduct **2d(1,4)**. However, **2d(1,2)** with the 1,2-dihydro pyridine structure was also produced in a 9% yield (eq 12).

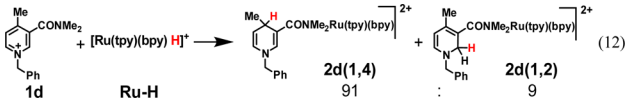

(12)

Because the reaction of **Ru-H** with **1d** was very slow, the formation of these adducts could be separately monitored by ^{1}H NMR. The main reason for the much slower rates than that of **1a−c** is the drastic increase in $\Delta H^{\ddagger}$ (Table 1). Interestingly, however, the decrease of the activation entropies of **2d(1,4)** ($\Delta S^{\ddagger}$ = −(6.76 ± 0.34) × 10 J mol^{-1} K^{-1}) and **2d(1,2)** ($\Delta S^{\ddagger}$ = −(7.46 ± 0.52) × 10 J mol^{-1} K^{-1}) were much smaller than the activation entropies of **2a(1,4)**, **2b(1,4)**, and **2c(1,4)** ($\Delta S^{\ddagger} \approx$ −100 J mol^{-1} K^{-1}). This indicates that approach of **Ru-H** to **1d** to form the transition state was much more difficult than that to **1a−c** because of synergistic effects of the steric hindrances of the methyl groups introduced into both the C-4 position and the carbamoyl group. The benzyl group at the C-1 position also had an important steric influence on transition state formation, which is discussed in more detail later. This suggests that the interactions of the hydride ligand with the C-4 position and the carbamoyl group with the Ru center, in the transition state between the reaction of **Ru-H** and **1d**, proceed at a distance longer than that in the cases of **1a−c**. This process likely governs the significantly greater adduct formation activation enthalpies from **1d** in comparison to **1b**. The **1d** transition states probably have looser conformations, which likely explain the loss in the hydride transfer C-4 position selectivity into the pyridinium moiety: i.e., the production of the byproduct **2d(1,2)**.

Some NAD(P)$^+$/NAD(P)H model compounds exhibiting a benzyl group at the N-1 position, e.g., **1a**, so-called BNA$^+$, have been used in many studies. To elucidate the substituent effect at the N-1 position, the reaction between **Ru-H** and **1e**, with methyl groups at both the N-1 and carbamoyl group, was compared with that between **Ru-H** and **1c**, which has a benzyl group at the N-1 position and a methyl group at the carbamoyl group. The reaction with **1e** produced **2e(1,4)** with a 1,4-dihydropyridine moiety as a main product. However, the isomer **2e(1,2)** with a 1,2-dihydropyridine moiety also formed as a byproduct. The ratio between the two during the reaction was [**2e(1,4)**]:[**2e(1,2)**] = 96:4 (eq 13).

The reaction rate for **1e** was approximately 1/8 slower at 300 K in comparison to that for **1c**. An increase in $\Delta H^{\ddagger}$ by 8.5 ± 0.3 kJ mol^{-1} in the reaction between **Ru-H** and **1e** mainly

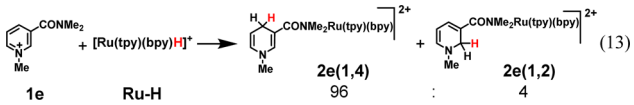

(13)

explains the decrease in the reaction rate in comparison with that for **1c** because of the stronger electron donating ability of the methyl group in comparison to the benzyl group. Note that the **2e(1,2)** adduct formed even though the corresponding adduct with the 1,2-dihydropyridine moiety was not produced from **1c** and that the introduction of the methyl group to the N-1 position should reduce the hydride-accepting ability of the carbon at the C-2 position, which is closer to the N-1 position than to the C-4 position. This result strongly indicates that a decrease in steric hindrance of a substituent at the N-1 position enables hydride transfer to the C-2 position. In other words, the steric hindrance of the benzyl group at the N-1 position plays an important role in the 1,4-selectivity during the hydride transfer reaction of **Ru-H** to the NAD(P)$^+$ model compounds. This was also supported by the fact that the decrease of $\Delta S^{\ddagger}$ in the reaction of **Ru-H** with **1e** (−(9.57 ± 0.07) × 10 J mol^{-1} K^{-1}) was relatively smaller than that with **1c** (−(1.07 ± 0.01) × 10^2 J mol^{-1} K^{-1}). Furthermore, we never detected the adduct with the 1,2-dihydropyridine moiety of the reaction between **Ru-H** and **1b**, although the methyl group was at the C-4 position of **1b**, which significantly lessens the hydride-accepting ability of the C-4 position. One of the main reasons for this is likely the steric hindrance of the benzyl group at the N-1 position.

In the reaction between **Ru-H** and **1f** with a 2,2,2-trifluoroethyl group, which is an electron-withdrawing group, at the N-1 position and two methyl groups at the carbamoyl group, the 1,2-dihydro adduct was produced along with the 1,4-dihydro adduct in the ratio [**2f(1,4)**]:[**2f(1,2)**] = 73:27 (eq 14).

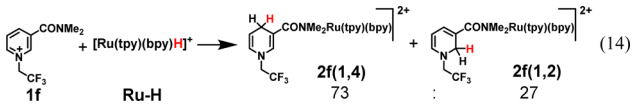

(14)

The reaction rate with **1f** was 21 times faster than that with **1c** at 300 K. The addition of the trifluoroethyl group to the N-1 position, instead of the benzyl group, should increase the hydride accepting ability, mainly of the C-2 position. This caused $\Delta H^{\ddagger}$ to be lower by 1.6 ± 0.3 k Jmol^{-1} in the case of **1f**. The ower − $T\Delta S^{\ddagger}$ value in the reaction of **1f** (25.9 ± 0.2 J mol^{-1}) in comparison with that of **1c** (32.0 ± 0.2 J mol^{-1}) more effectively promoted the increase in the reaction rate at 300 K. An increase in a degree of freedom in the transition state, which can give both **2f(1,4)** and **2f(1,2)**, should increase the activation entropy of the reaction. A similar analysis can be more clearly conducted in a comparison of reactivity between **1f** and **1a**. Although $\Delta H^{\ddagger}$ of the reaction between **Ru-H** and **1f** was as large as that for **1a**, the reaction rate with **1f** was 4 times faster than that with **1a** at 300 K. This can be explained if we consider that the adduct with the 1,4-dihydropyridine moiety was only produced in the case of **1a**. For **1f**, the adduct having the 1,2-dihydropyridine moiety was produced in approximately 30% yield, which reduced $-T\Delta S^{\ddagger}$.

The main product was the 1,2-adduct **2g(1,2)** in the case of **1g**, which exhibited a trifluoroethyl group at the N-1 position and a methyl group at the C-4 position (eq 15). This high **2g(1,2)** yield may be caused by a number of reasons, including less steric hindrance of the trifluoroethyl group at the N-1 position, the electron-withdrawing ability of the trifluoroethyl

DOI: 10.1021/acs.organomet.5b00713
Organometallics XXXX, XXX, XXX−XXX

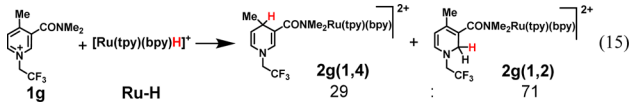

(15)

group, and steric and electronic effects of the methyl group at the C-4 position, which should cause a slower hydride transfer rate to the C-4 position. The transition state leading to the 1,2-dihydro adduct likely had a more compact structure than the transition states leading to **2d(1,4)** and **2d(1,2)** formation, owing to the lesser steric hindrance of the trifluoroethyl group in comparison to that of the benzyl group, which probably enhances the $-T\Delta S^{\ddagger}$ value in the **1g** reaction in comparison with that in the **1d** reaction. Excluded volumes of two model compounds having the benzyl (**1c**) and CH_2CF_3 (**1f**) groups at the 1-positions in DMF were calculated as 2573 and 1541 Å^3, respectively, with the assumption that they are freely rotating. This is also supported by the fact that the benzyl group gave greater steric repulsion than the CH_2CF_3 group.

The introduction of another methyl group to the C-2 position drastically affected the product distribution. For the **1h** molecule with methyl groups at the C-2, C-4, and carbamoyl group positions, where the difference in comparison with **1g** was just the methyl substituent at the C-2 position, the main product was the 1,4-dihydro adduct with 96% selectivity (eq 16).

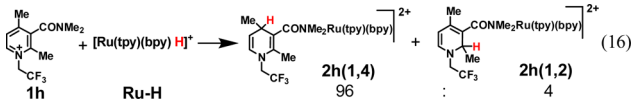

(16)

The introduction of an electron-donating methyl group made the hydride insertion less feasible, particularly to the C-2 position.

Interestingly, the $-T\Delta S^{\ddagger}$ value of the reaction with **1h** was similar to that with **1g** but much larger than that with **1d**, although its product distribution was similar to that with **1h**. This also suggests something about the properties of the benzyl group at the N-1 position. For **1d**, the benzyl group at the N-1 position and the methyl groups at the C-4 position and on the carbamoyl group efficiently prevented **1d** from approaching **Ru-H** in the transition state, which induced a $-T\Delta S^{\ddagger}$ value significantly smaller than that for the other NAD(P)$^+$ model compounds. On the other hand, such an effect was not observed in the case of **1h**, which has methyl groups not only at the C-4 position and carbamoyl group but also at the C-2 position. This strongly indicates that the benzyl group at the N-1 position hindered the approach by **Ru-H** in the transition state.

Cleavage Reaction of the Adducts 2. The 1:1 adducts (**2**) produced via the reactions of **Ru-H** with each NAD(P)$^+$ model compound **1** were cleaved and yielded the corresponding dihydro products, and the Ru complex coordinated to the solvent quantitatively (eqs 17 and 18).

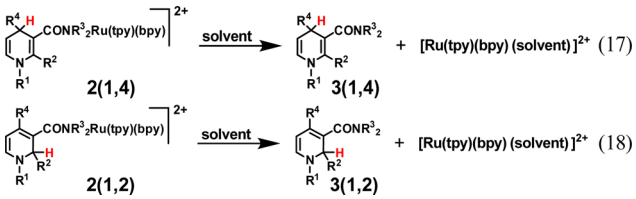

(17)
(18)

All types of **2** produced by the reactions between **1** and **Ru-H**, except **2g**, were quantitatively separated into the corresponding dihydronicotinamide derivative and the solvent complex for several hours, up to around 20 h. Initially, only **2(1,4)** was produced from **1a–c**, following which only the corresponding 1,4-dihydronicotinamide **3(1,4)** was obtained (eq 17). Other cases (**1d–f,h**) produced both the 1,2- and 1,4-adducts. The corresponding 1,2- and 1,4-dihydronicotinamides **3(1,2)** and **3(1,4)** were produced in the same relative amounts as the adducts (Table 1). Therefore, during the cleavage reactions, isomerization of the dihydronicotinamide moiety should not proceed. Only one exceptional case was the reaction of **1g** with **Ru-H**, whereby the ratio of the adducts was [**2g(1,4)**]:[**2g(1,2)**] = 29:71, whereas [**3g(1,4)**]:[**3g(1,2)**] = 43:57 (Figure 7). Because these ratios did not change during the reaction, the following two kinetic explanations for the cleavage reactions of **2g(1,4)** and **2g(1,2)** might be considered.

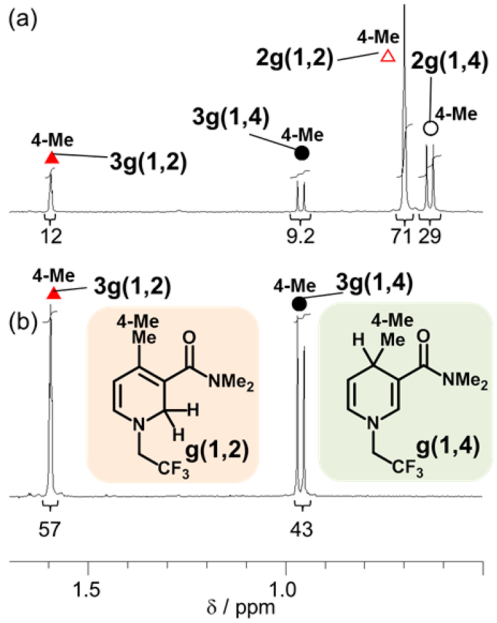

Figure 7. ^{1}H NMR spectra of the methyl group at the C-4 position of the dihydronicotinamide moiety at (a) 10 min and (b) 20 h after mixing **1g** (8.4 mM) with **Ru-H** (8.0 mM) in an MeCN-d_3 solution at room temperature: (red △) **2g(1,2)**; (black ○) **2g(1,4)**; (red ▲) **3g(1,2)**; (black ●) **3g(1,4)**.

(1) Rapid isomerization between **2g(1,4)** and **2g(1,2)** occurred within the ^{1}H NMR measurements, and the cleavage reactions of each adduct proceeded with different reaction rates.
(2) Following adduct cleavage, chemical equilibrium between **3g(1,4)** and **3g(1,2)** was achieved within the time scale of the ^{1}H NMR measurements because of their rapid isomerization.

CONCLUSION

Formation processes of the 1:1 adducts (**2**) by the reactions of various NAD(P)$^+$ model compounds (**1**) with **Ru-H** were discussed in detail using production distributions, kinetics, and activation parameters. The main reason the hydride did not transfer to the C-6 position from **Ru-H** is that, in the transition state for the production of **2**, the interaction between the Ru center and the carbamoyl group of **1** played an important role and this interaction promotes the hydride ligand to a location unfavorable for interaction with the carbon at the C-6 position. One of the primary factors leading to the formation of the 1,4-dihydro isomer of the NAD(P)H model compound (**3**) as the

DOI: 10.1021/acs.organomet.5b00713
Organometallics XXXX, XXX, XXX–XXX

final product is the steric hindrance of the benzyl group at the N-1 position of **1**, which prevents hydride transfer to the carbon at the C-2 position. When a methyl group was introduced into the pyridinium ring at the C-4 and/or C-2 positions, the reaction rate drastically decreased, mainly because decreasing the electrophilic character of the carbon at the position increased $\Delta H^{\ddagger}$ for the formation of **2**. In addition, the steric hindrance of the substituents significantly decreased the reaction rate because of the separation of **Ru-H** from **1** in the transition state, and this distance affected the product distribution in **2**.

EXPERIMENTAL SECTION

General Procedures. ^{1}H and ^{13}C NMR spectra were recorded on a JEOL AL300, AL400, or ECAII400 or Bruker AC500 spectrometer. The residual proton of the deuterated solvent was used as an internal standard. Melting points were measured using a Stuart Scientific Co. Ltd. SMP3 melting point apparatus. Measurements using stopped-flow techniques were performed on a Union Giken RA-401 stopped-flow spectrophotometer combined with an Otsuka Electronic Co. MCPD-5000 or MCPD-9000 multichannel photodiode array system. Changes in both absorbance at 535 nm (recorded using the stopped-flow method) and peaks attributed to the product (observed in the ^{1}H NMR spectra) with the passage of time were analyzed using Igor Pro 6 (WaveMetrics, Inc.) and Mathematica 9.0 (Wolfram) programs.

Materials. *N*,*N*-Dimethylformamide (DMF) and DMF-d_7 were dried over molecular sieves 4A and then distilled under reduced pressure (10−20 mmHg). All other reagents were reagent-grade quality and were used without further purification. [Ru(tpy)(bpy)H](PF$_6$) (**Ru-H**),[12] 3-carbamoyl-4-methylpyridine,[13] 1-benzyl-3-carbamoylpyridinium hexafluorophosphate (**1a**),[14] and 2,4-dimethyl-3-carboxypyridine hydrochloride were prepared according to the reported methods.

Syntheses. *1-Benzyl-3-carbamoyl-4-methylpyridinium Hexafluorophosphate (**1b**).* A 15 mL MeCN solution containing 4-methylnicotinamide (267 mg, 1.96 mmol) and 2 mL of benzyl chloride was refluxed for 18 h. After a small amount of diethyl ether was added to the solution, the precipitated brown solids were filtered and then dissolved in ethanol. The solution was treated with charcoal. After the solvent was evaporated, the residue was dissolved in a small amount of water and a NH_4PF_6-saturated aqueous solution was added dropwise. The precipitates were recrystallized with water. The yield was 61% (445 mg, 1.19 mmol). Mp: 133 °C. Anal. Calcd for $C_{14}H_{15}F_6N_2OP$: C. 45.17; H. 4.06; N. 7.53. Found: C. 45.26; H. 3.95; N. 7.51. ^{1}H NMR (298 MHz, MeCN-d_3): δ (ppm) 8.74 (s, 1H, 2-H), 8.56 (d, J = 5.1 Hz, 1H, 6-H), 7.88 (m, 5H, Ph), 7.28 (d, J = 5.1 Hz, 1H, 5-H), 6.78 (s, 1H, NH$_2$), 6.58 (s, 1H, NH$_2$), 5.63 (s, 2H, 1-CH$_2$−), 2.65 (s, 3H, 4-Me). ^{13}C NMR (101 MHz, MeCN-d_3): δ (ppm) 165.3 (C═O), 159.5 (4-C), 144.7 (6-C), 143.2 (2-C), 137.5 (3-C), 133.8 (Ph), 131.4 (5-C), 130.9 (Ph), 130.5 (Ph), 130.1 (Ph), 64.9 (1-CH$_2$−), 20.8 (4-Me).

*1-Benzyl-3-(N,N-dimethylcarbamoyl)pyridinium Hexafluorophosphate (**1c**).* An MeCN solution (2 mL) containing *N*,*N*-dimethylnicotinamide (1.00 g, 6.66 mmol) and benzyl chloride (1.00 mg, 7.10 mmol) was refluxed for 12 h. After the solvent was evaporated, the residue was dissolved into a small amount of water. An NH_4PF_6-saturated aqueous solution was dropped to the solution. The white precipitates were recrystallized with water. The yield was 80% (2.05 g, 5.31 mmol). Mp: 164 °C. Anal. Calcd for $C_{15}H_{17}F_6N_2OP$: C, 46.64; H, 4.44; N, 7.25. Found: C, 46.78; H, 4.15; N, 7.29. ^{1}H NMR (298 MHz, MeCN-d_3): δ (ppm) 8.80 (s, 1H, 2-H), 8.74 (d, J = 6.4 Hz, 1H, 6-H), 8.50 (d, J = 7.8 Hz, 1H, 4-H), 8.06 (dd, J = 7.8, 6.4 Hz, 1H, 5-H), 7.49 (m, 5H, Ph), 5.73 (s, 2H, 1-CH$_2$−), 3.05 (s, 3H, NMe$_2$), 2.91 (s, 3H, NMe$_2$). ^{13}C NMR (101 MHz, MeCN-d_3): δ (ppm) 164.7 (C═O), 145.7 (6-C), 145.2 (4-C), 144.1 (2-C), 138.4 (3-C), 133.4 (Ph), 131.1 (Ph), 130.6 (Ph), 130.5 (Ph), 129.7 (5-C), 65.8 (1-CH$_2$−), 39.6 (NMe$_2$), 35.7 (NMe$_2$).

3-(N,N-Dimethylcarbamoyl)-4-methylpyridine. A DMF solution (12 mL) containing 3-carbamoyl-4-methylpyridine (1.00 g, 7.35 mmol) and sodium hydride (528 mg, 22.0 mmol) was stirred at 0 °C for 1 h, and iodomethane (2.30 g, 16.1 mmol) was added. The solution was warmed to room temperature and stirred for 2 h. The solution was poured into 40 mL of water, followed by extraction (3 × 30 mL) with CH_2Cl_2. The organic layer was dried with anhydrous sodium sulfate and evaporated. After the solvent was evaporated, the target compound was distilled under low pressure (111 °C at 0.3 mmHg) as a colorless oil. The yield was 23% (276 mg, 1.68 mmol). ^{1}H NMR (400 MHz, MeCN-d_3): δ (ppm) 8.44 (d, J = 5.0 Hz, 1H, 6-H), 8.33 (s, 1H, 2-H), 7.23 (d, J = 5.0 Hz, 1H, 5-H), 3.05 (s, 3H, NMe$_2$), 2.79 (s, 3H, NMe$_2$), 2.25 (s, 3H, 4-Me). ^{13}C NMR (101 MHz, MeCN-d_3): δ (ppm) 169.2 (C═O), 150.4 (6-C), 147.4 (2-C), 144.7 (4-C), 134.5 (3-C), 126.2 (5-C), 38.7 (NMe$_2$), 34.7 (NMe$_2$), 18.6 (4-Me).

*1-Benzyl-3-(N,N-dimethylcarbamoyl)-4-methylpyridinium Hexafluorophosphate (**1d**).* This compound was synthesized using a method similar to that used for **1c**, but instead of using *N*,*N*-dimethylnicotinamide, 3-(*N*,*N*-dimethylcarbamoyl)-4-methylpyridine was used. The yield was 81% (596 mg, 1.49 mmol). Mp: 190 °C dec. Anal. Calcd for $C_{16}H_{19}F_6N_2OP$: C, 48.01; H, 4.78; N, 7.00. Found: C, 47.75; H,4.68; N, 7.10. ^{1}H NMR (298 MHz, MeCN-d_3): δ (ppm) 8.56 (d, J = 6.6 Hz, 1H, 6-H), 8.55 (s, 1H, 2-H), 7.88 (d, J = 6.6 Hz, 1H, 5-H), 7.51−7.40 (m, 5H, Ph), 5.64 (s, 2H, 1-CH$_2$−), 3.06 (s, 3H, NMe$_2$), 2.79 (s, 3H, NMe$_2$), 2.52 (s, 3H, 4-Me). ^{13}C NMR (101 MHz, MeCN-d_3): δ (ppm) 164.3 (C═O), 158.0 (4-C), 144.2 (6-C), 141.9 (2-C), 138.6 (3-C), 133.7 (Ph), 131.2 (5-C), 130.9 (Ph), 130.5 (Ph), 130.3 (Ph), 65.0 (1-CH$_2$−), 38.7 (NMe$_2$), 35.1 (NMe$_2$), 20.1 (4-Me).

*1-Methyl-3-(N,N-dimethylcarbamoyl)pyridinium Hexafluorophosphate (**1e**).* A 3 mL MeCN solution containing 3-(*N*,*N*-dimethylcarbamoyl)-4-methylpyridine (2.0 g, 13.3 mmol) and iodomethane (3.06 g, 21.6 mmol) were refluxed for 13 h. After the solvent was evaporated, the residue was dissolved into a small amount of methanol, followed by dropping a saturated methanol solution of NH_4PF_6. The white precipitates were recrystallized with methanol/ethanol. The yield was 57% (2.37 g, 7.64 mmol). Mp: 124−125 °C. Anal. Calcd for $C_9H_{13}F_6N_2OP$: C, 34.85; H, 4.22; N, 9.03. Found: C, 34.84; H, 4.00; N, 8.94. ^{1}H NMR (400 MHz, MeCN-d_3): δ (ppm) 8.69 (s, 1H, 2-H), 8.63 (d, J = 6.4 Hz, 1H, 6-H), 8.47 (d, J = 8.1 Hz, 1H, 4-H), 8.04 (dd, J = 6.4, 8.1 Hz, 1H, 5-H), 4.30 (d, J = 8.1 Hz, 3H, 1-Me), 3.07 (s, 3H, NMe$_2$), 2.94 (s, 3H, NMe$_2$). ^{13}C NMR (101 MHz, MeCN-d_3): δ (ppm) 164.8 (C═O), 146.6 (6-C), 145.0 (2-C), 144.4 (4-C), 138.0 (3-C), 129.2 (5-C), 49.5 (1-Me), 39.6 (NMe$_2$), 35.7 (NMe$_2$).

*1-(2,2,2-Trifluoroethyl)-3-(N,N-dimethylcarbamoyl)pyridinium Hexafluorophosphate (**1f**).* A 2 mL MeCN solution containing *N*,*N*-dimethylnicotinamide (1.00 g, 6.66 mmol) and 2,2,2-trifluoroethyl trifluoromethanesulfonate (1.90 g, 8.19 mmol) was refluxed for 12 h. After the solvent was evaporated, the residue was dissolved into a small amount of water, followed by dropping a saturated aqueous solution of NH_4PF_6. The white precipitates were recrystallized with water. The yield was 87% (2.19 g, 5.79 mmol). Mp: 182−183 °C. Anal. Calcd for $C_{10}H_{15}F_6N_2OP$: C, 31.76; H, 3.20; N, 7.41. Found: C, 31.66; H, 3.36; N, 7.41. ^{1}H NMR (298 MHz, MeCN-d_3): δ (ppm) 8.87 (s, 1H, 2-H), 8.80 (d, J = 6.2 Hz, 1H, 6-H), 8.70 (d, J = 8.0 Hz, 1H, 4-H), 8.22 (dd, J = 8.0, 6.2 Hz, 1H, 5-H), 5.36 (q, J = 7.9 Hz, 2H, 1-CH$_2$−), 3.07 (s, 3H, NMe$_2$), 2.97 (s, 3H, NMe$_2$). ^{13}C NMR (101 MHz, MeCN-d_3): δ (ppm) 164.1 (C═O), 147.6 (4-C), 147.5 (6-C), 146.1 (2-C), 139.0 (3-C), 130.4 (5-C), 123.0 (q, J_{C-F} = 280 Hz, CF$_3$), 60.6 (q, J_{C-F} = 36 Hz, 1-CH$_2$−), 39.7 (NMe$_2$), 35.8 (NMe$_2$).

*1-(2,2,2-Trifluoroethyl)-3-(N,N-dimethylcarbamoyl)-4-methylpyridinium Hexafluorophosphate (**1g**).* 3-(*N*,*N*-Dimethylcarbamoyl)-4-methylpyridine (276 mg, 2.02 mmol) was dissolved in 2,2,2-trifluoroethyl trifluoromethanesulfonate (1.88 mg, 8.11 mmol), and the solution was heated to 100 °C for 12 h. The following processes were the same as those for **1f**. The yield was 52% (411 mg, 1.05 mmol). Mp: 199−200 °C dec. Anal. Calcd for $C_{17}H_{18}F_9N_2OP$: C, 33.69; H, 3.60; N, 7.1. Found: C, 33.68; H, 3.60; N, 7.04. ^{1}H NMR (400 MHz, MeCN-d_3): δ (ppm) 8.61 (d, J = 6.8 Hz, 1H, 6-H), 8.60 (s, 1H, 2-H), 8.04 (d, J = 6.8 Hz, 1H, 5-H), 5.26 (q, J = 8.1 Hz, 2H, 1-CH$_2$−), 3.09 (s, 3H, NMe$_2$), 2.85 (s, 3H, NMe$_2$), 2.60 (s, 3H, 4-Me). ^{13}C NMR (101 MHz, MeCN-d_3): δ (ppm) 163.6 (C═O), 161.2 (4-C), 145.8 (6-C), 143.5 (2-C), 139.0 (3-C), 132.0 (5-C), 123.1 (q, J_{C-F} = 280 Hz, CF$_3$), 60.0 (q, J_{C-F} = 35 Hz, 1-CH$_2$−), 38.7 (NMe$_2$), 35.2 (NMe$_2$), 20.6 (4-Me).

DOI: 10.1021/acs.organomet.5b00713
Organometallics XXXX, XXX, XXX−XXX

2,4-Dimethyl-3-(N,N-dimethylcarbamoyl)pyridine. 2,4-Dimethyl-3-carboxypyridine hydrochloride (2.43 g, 13.0 mmol) was dissolved in thionyl chloride (13 mL), and the solution was heated to 80−90 °C for 1 h. After thionyl chloride was evaporated under reduced pressure (12 mmHg at 80 °C), the residue was dissolved in a mixed dichloromethane (5 mL) and triethylamine (4.4 mL) solution. A THF solution (7 mL) containing dimethylamine (13.1 mmol) was added dropwise to the mixed solution for 20 min and then stirred for 1.5 h at room temperature. After evaporation of the solvent, the residue was dissolved in a 35% HCl aqueous solution (11.3 mL). Active charcoal was added to the solution, and the solution was heated for about 2 min. After the active charcoal was filtered out, the filtrate was neutralized with $NaHCO_3$ up to pH 7, and the compound was extracted with dichloromethane four times. The combined organic layer was washed with an aqueous solution containing $NaHCO_3$. The solution was dried over Na_2SO_4 and then evaporated under reduced pressure. The colorless oil was obtained by distillation under reduced pressure (0.5 mmHg, at 100 °C). The yield was 77% (1.79 g, 10.0 mmol). ^{1}H NMR (400 MHz, MeCN-d_3): δ (ppm) 8.31 (d, J = 5.1 Hz, 1H, 6-H), 7.04 (d, J = 5.1 Hz, 3H, 5-H), 3.06 (s, 3H, NMe_2), 2.75 (s, 3H, NMe_2), 2.34 (s, 3H, 2-Me), 2.18 (s, 3H, 4-Me). ^{13}C NMR (101 MHz, MeCN-d_3): δ (ppm) 169.7 (C═O), 154.3 (2-C), 149.4 (6-C), 144.1 (4-C), 133.5 (3-C), 123.5 (5-C), 37.6 (NMe_2), 34.2 (NMe_2), 22.2 (2-Me), 18.6 (4-Me).

*1-(2,2,2-Trifluoroethyl)-2,4-methyl-3-(N,N-dimethylcarbamoyl)-pyridinium Hexafluorophosphate (**1h**).* 2,4-Dimethyl-3-(*N*,*N*-dimethylcarbamoyl)pyridine (600 mg, 3.37 mmol) was dissolved in 2,2,2-trifluoroethyl trifluoromethanesulfonate (2.35 g, 10.1 mmol), and the solution was heated to 100 °C for 14 h. The following processes were the same as those for **1f**. The yield was 31% (430 mg, 1.20 mmol). Mp: 203−204 °C dec. Anal. Calcd for $C_{12}H_{16}F_9N_2OP$: C, 35.48; H, 3.97; N, 6.90. Found: C, 35.68; H, 3.90; N, 6.94. ^{1}H NMR (400 MHz, MeCN-d_3): δ (ppm) 8.51 (d, J = 6.7 Hz, 1H, 6-H), 7.86 (d, J = 6.7 Hz, 1H, 5-H), 5.28 (qd, J = 8.0, 2.0 Hz, 2H, 1-CH_2−), 3.11 (s, 3H, NMe_2), 2.80 (s, 3H, NMe_2), 2.68 (s, 3H, 2-Me), 2.52 (s, 3H, 4-Me). ^{13}C NMR (MeCN-d_3, 101 MHz): δ (ppm) 164.7 (C═O), 159.9 (4-C), 153.6 (2-C), 146.5 (6-C), 139.9 (3-C), 129.2 (5-C), 123.4 (q, J_{CF} = 280 Hz, CF_3), 56.9 (q, J_{CF} = 35 Hz, 1-CH_2−), 37.7 (NMe_2), 34.8 (NMe_2), 20.8 (4-Me), 18.6 (2-Me).

Pursuit of the Reaction between the NAD(P)$^+$ Model Compound and Ru-H. *^{1}H NMR Spectroscopy Analysis.* An MeCN-d_3 solution (0.5 mL) was bubbled with Ar in an NMR tube for 30 min, and **Ru-H** (4.0 μmol) and an NAD(P)$^+$ model compound (4.2 μmol) were then dissolved in it, while the mixture was continuously bubbled with Ar. The reaction solution was bubbled with Ar for an additional 5 min. After the solution was kept in the dark for a suitable time period, the ^{1}H NMR spectrum was measured. This procedure was repeated until the formation of the corresponding NAD(P)H model compound or compounds was completed.

Determination of Rate Constants. For stopped-flow measurements, each DMF solution containing **Ru-H** (0.031 mM) or the NAD(P)$^+$ model compound (0.38 mM) was bubbled with Ar for 20 min. These solutions were instantaneously mixed using the stopped-flow apparatus, where the initial concentrations of **Ru-H** ([**Ru-H**]$_{int}$) and the NAD(P)$^+$ model compound ([**1**]$_{int}$) were 0.0155 and 1.9 mM, respectively. After mixing, UV−vis absorption spectral changes in the reaction solution were obtained using a photodiode detector in the cases of **1b**,**g**,,**h** or the absorbance at 535 nm was obtained using a photomultiplier detector for relatively fast reaction (**1a**,**c**,**e**,**f**). The same experiments were repeated 6−30 times, and the data were well fitted using a single exponential function. For details, see the Supporting Information.

For determining the reaction rate of **1d** with **Ru-H**, each 0.5 mL of DMF-d_7 solution containing **1d** (8 mM) or **Ru-H** (8 mM) was mixed under an Ar atmosphere, and the mixed solutions were kept at each temperature. Second-order kinetics was directly applied to obtain k using the ^{1}H NMR data. The global fitting method was used with the average integration values of the peaks at 9.81 and 8.68 ppm for decrease of **Ru-H** and those of the peaks for formation and decrease of **2d(1,4)** (5.78, 5.64, 3.96, and 0.64 ppm), **2d(1,2)** (6.24 and 0.78 ppm), **3d(1,4)** (6.46, 6.05, 4.58, 4.43, 2.97, and 0.94 ppm), and **3d(1,2)** (4.18, 3.72, and 1.59 ppm) (Figure 6). The total yields of **2d** and **3d** were about 90% on the basis of **Ru-H** consumed during the reaction.

Computational Calculations. All quantum chemical calculations were carried out using the ORCA program package (version 3.0.3).[15] Geometry optimizations under implicit solvation were carried out using density functional theory (DFT) with the spin-restricted PW6B95 hybrid meta-GGA functional,[16] which was supplemented with the atom-pairwise dispersion correction with Becke-Johnson damping (D3BJ).[17] In SCF and gradient calculations, a combination (RIJCOSX)[18] of the "resolution of the identity" approximation[19] for the Coulomb parts and the "chain-of-spheres exchange" algorithm for the exchange parts were employed in order for the efficient computation of the Fock matrix. The single polarized double-ζ basis set (def2-SVP)[20] was used along with an appropriate density-fitting basis set (def2-SVP/J)[21] for C, H, N, and O atoms. For the Ru atom, the single polarized double-ζ valence basis set (def2-SVP)[20] along with the corresponding density-fitting basis set (def2-SVP/J)[21] were accompanied by the Stuttgart−Dresden effective core potentials (ECP, 28MWB)[22] for taking the relativistic effect into account. Implicit solvation by DMF was implemented in a dielectric continuum (ε = 38.30, n = 1.430) using a conductor-like screening model (COSMO).[23] All local stationary structures were confirmed by numerical vibrational frequency calculations, using the same level of the theory as for the geometry optimizations. For their Gibbs energies, electronic SCF energies were calculated first at the geometries optimized by the above method, but using the single polarized triple-ζ basis set (def2-TZVP)[20] along with an appropriate density-fitting basis set (def2-TZVP/J)[21] for C, H, N, and O atoms and the single polarized triple-ζ valence basis set (def2-TZVP)[20] with the corresponding density-fitting basis set (def2-TZVP/J)[21] under the same ECP (28MWB) for the Ru atom. Each of the Gibbs free energies was calculated by addition of this electronic SCF energy to a zero-point energy, thermal corrections, and entropy terms calculated using the vibrational calculations under the ideal gas, rigid rotor, and harmonic oscillator approximations at a temperature and pressure of 298.15 K and 1 atm, respectively. In the case of adducts, they were finally corrected by the counterpoise method of Boys and Bernardi[24] to compensate for the basis set superposition error (BSSE) between the [Ru(tpy)(bpy)]$^{2+}$ and dihydropyridine moieties. For evaluating the excluded volume of a solvent (DMF) by a substituent at the N-1 position of a NAD(P)$^+$ model, a solvent-accessible surface of a molecule, where each atom has its own vdW radius, by DMF (effective radius 2.64 Å) was calculated by employing the Winmostar program (version 5.003) at a geometry optimized by the above method. Then, a series of such surfaces was calculated at the geometries optimized except a dihedral angle defined by the pyridine ring and the substituent, where these angles were varied from 0° to 360° with an interval of 20°. Finally, an envelope of this series of the surfaces was taken as the excluded volume.

■ ASSOCIATED CONTENT

Supporting Information

The Supporting Information is available free of charge on the ACS Publications website at DOI: 10.1021/acs.organomet.5b00713.

Derivation of eq 6 and rate constants, ^{1}H NMR spectra, UV−vis spectra, decays of the absorbance, Eyring plots, and most stable structures of **2a**,**c** calculated using the DFT method (PDF)

■ AUTHOR INFORMATION

Corresponding Author

*E-mail for O.I.: ishitani@chem.titech.ac.jp.

Notes

The authors declare no competing financial interest.

DOI: 10.1021/acs.organomet.5b00713
Organometallics XXXX, XXX, XXX−XXX

■ ACKNOWLEDGMENTS

This work was partially supported by a Grant-in-Aid for Scientific Research on Innovative Areas "Artificial photosynthesis (AnApple)" (No. 24107005).

■ REFERENCES

(1) (a) Batie, C. J.; Kamin, H. *J. Biol. Chem.* **1984**, *259*, 11976−11985. (b) Karplus, P. A.; Bruns, C. M. *J. Bioenerg. Biomembr.* **1994**, *26*, 89−99. (c) Carrillo, N.; Ceccarelli, E. A. *Eur. J. Biochem.* **2003**, *270*, 1900−1915. (d) Karplus, P. A.; Faber, H. R. *Photosynth. Res.* **2004**, *81*, 303−315. (e) Medina, M. *FEBS J.* **2009**, *276*, 3942−3958.

(2) (a) Dołęga, A. *Coord. Chem. Rev.* **2010**, *254*, 916−937. (b) Plapp, B. V. *Arch. Biochem. Biophys.* **2010**, *493*, 3−12.

(3) (a) Paglietti, G. S. P.; Nuvole, A.; Soccolini, F.; Acheson, R. M. *J. Chem. Res. Miniprint* **1983**, 2326−2342. (b) Eisner, U.; Kuthan, J. *Chem. Rev.* **1972**, *72*, 1−42. (c) Stout, D. M.; Meyers, A. I. *Chem. Rev.* **1982**, *82*, 223−243. (d) Lavilla, R. *J. Chem. Soc., Perkin Trans. 1* **2002**, 1141−1156. (e) Wagenknecht, P. S.; Sambriski, E. J. *Recent Res. Dev. Inorg. Chem.* **2003**, *3*, 35−50. (f) McSkimming, A.; Colbran, S. B. *Chem. Soc. Rev.* **2013**, *42*, 5439−5488. (g) Quinto, T.; Köhler, V.; Ward, T. R. *Top. Catal.* **2014**, *57*, 321−331.

(4) (a) Soldevila-Barreda, J. J.; Bruijnincx, P. C. A.; Habtemariam, A.; Clarkson, G. J.; Deeth, R. J.; Sadler, P. J. *Organometallics* **2012**, *31*, 5958−5967. (b) Maenaka, Y.; Suenobu, T.; Fukuzumi, S. *J. Am. Chem. Soc.* **2012**, *134*, 9417−9427. (c) Maenaka, Y.; Suenobu, T.; Fukuzumi, S. *J. Am. Chem. Soc.* **2012**, *134*, 367−374. (d) Haquette, P.; Talbi, B.; Barilleau, L.; Madern, N.; Fosse, C.; Salmain, M. *Org. Biomol. Chem.* **2011**, *9*, 5720−5727. (e) Canivet, J.; Suss-Fink, G.; Stepnicka, P. *Eur. J. Inorg. Chem.* **2007**, *2007*, 4736−4742. (f) Yan, Y. K.; Melchart, M.; Habtemariam, A.; Peacock, A. F.; Sadler, P. J. *JBIC, J. Biol. Inorg. Chem.* **2006**, *11*, 483−488.

(5) (a) Ruppert, R.; Herrmann, S.; Steckhan, E. *J. Chem. Soc., Chem. Commun.* **1988**, 1150−1151. (b) Steckhan, E.; Herrmann, S.; Ruppert, R.; Dietz, E.; Frede, M.; Spika, E. *Organometallics* **1991**, *10*, 1568−1577. (c) Lo, H. C.; Buriez, O.; Kerr, J. B.; Fish, R. H. *Angew. Chem., Int. Ed.* **1999**, *38*, 1429−1432. (d) Lo, H. C.; Leiva, C.; Buriez, O.; Kerr, J. B.; Olmstead, M. M.; Fish, R. H. *Inorg. Chem.* **2001**, *40*, 6705−6716.

(6) Kobayashi, A.; Konno, H.; Sakamoto, K.; Sekine, A.; Ohashi, Y.; Iida, M.; Ishitani, O. *Chem. - Eur. J.* **2005**, *11*, 4219−4226.

(7) (a) Ishitani, O.; Inoue, N.; Koike, K.; Ibusuki, T. *J. Chem. Soc., Chem. Commun.* **1994**, 367. (b) Kobayashi, A.; Takatori, R.; Kikuchi, I.; Konno, H.; Sakamoto, K.; Ishitani, O. *Organometallics* **2001**, *20*, 3361−3363. (c) Matsubara, Y.; Konno, H.; Kobayashi, A.; Ishitani, O. *Inorg. Chem.* **2009**, *48*, 10138−10145. (d) Matsubara, Y.; Koga, K.; Kobayashi, A.; Konno, H.; Sakamoto, K.; Morimoto, T.; Ishitani, O. *J. Am. Chem. Soc.* **2010**, *132*, 10547−10552.

(8) (a) Ohno, A.; Ikeguchi, M.; Kimura, T.; Oka, S. *J. Am. Chem. Soc.* **1979**, *101*, 7036−7040. (b) Ohno, A.; Goto, T.; Nakai, J.; Oka, S. *Bull. Chem. Soc. Jpn.* **1981**, *54*, 3478−3481. (c) Meyers, A. I.; Oppenlaender, T. *J. Am. Chem. Soc.* **1986**, *108*, 1989−1996. (d) Meyers, A. I.; Brown, J. D. *J. Am. Chem. Soc.* **1987**, *109*, 3155−3156. (e) De Kok, P. M. T.; Bastiaansen, L. A. M.; Van Lier, P. M.; Vekemans, J. A. J. M.; Buck, H. M. *J. Org. Chem.* **1989**, *54*, 1313−1320. (f) Okamura, M.; Mikata, Y.; Yamazaki, N.; Tsutsumi, A.; Ohno, A. *Bull. Chem. Soc. Jpn.* **1993**, *66*, 1191−1196. (g) Mikata, Y.; Hayashi, K.; Mizukami, K.; Matsumoto, S.; Yano, S.; Yamazaki, N.; Ohno, A. *Tetrahedron Lett.* **2000**, *41*, 1035−1038. (h) Mikata, Y.; Aida, S.; Yano, S. *Org. Lett.* **2004**, *6*, 2921−2924.

(9) In a DMF-d_7 solution instead of MeCN-d_3, a similar experiment was examined. The ratio was [**3d(1,4)**]:[**3d(1,2)**] = 91:9, which was very similar to that obtained in MeCN-d_3 solution.

(10) The coordinating atom to the Ru(II) center, i.e., N or O, has not yet been determined in the transition state.

(11) Matsubara, Y.; Kosaka, T.; Koga, K.; Nagasawa, A.; Kobayashi, A.; Konno, H.; Creutz, C.; Sakamoto, K.; Ishitani, O. *Organometallics* **2013**, *32*, 6162−6165.

(12) Konno, H.; Sakamoto, K.; Ishitani, O. *Angew. Chem., Int. Ed.* **2000**, *39*, 4061−4063.

(13) Bobbitt, J. M.; Scola, D. A. *J. Org. Chem.* **1960**, *25*, 560−564.

(14) Fukuzumi, S.; Kondo, Y.; Tanaka, T. *J. Chem. Soc., Perkin Trans. 2* **1984**, 673−679.

(15) Neese, F. *Wiley Interdiscip. Rev.: Comput. Mol. Sci.* **2012**, *2*, 73−78.

(16) (a) Zhao, Y.; Truhlar, D. G. *J. Phys. Chem. A* **2005**, *109*, 5656−5667. (b) Goerigk, L.; Grimme, S. *Phys. Chem. Chem. Phys.* **2011**, *13*, 6670−6688.

(17) (a) Grimme, S.; Antony, J.; Ehrlich, S.; Krieg, H. *J. Chem. Phys.* **2010**, *132*, 154104. (b) Grimme, S.; Ehrlich, S.; Goerigk, L. *J. Comput. Chem.* **2011**, *32*, 1456−1465.

(18) Neese, F.; Wennmohs, F.; Hansen, A.; Becker, U. *Chem. Phys.* **2009**, *356*, 98−109.

(19) Neese, F. *J. Comput. Chem.* **2003**, *24*, 1740−1747.

(20) Weigend, F.; Ahlrichs, R. *Phys. Chem. Chem. Phys.* **2005**, *7*, 3297−3305.

(21) Weigend, F. *Phys. Chem. Chem. Phys.* **2006**, *8*, 1057−1065.

(22) (a) Andrae, D.; Haussermann, U.; Dolg, M.; Stoll, H.; Preuss, H. *Theor. Chim. Acta* **1990**, *77*, 123−141. (b) Flores-Moreno, R.; Alvarez-Mendez, R. J.; Vela, A. K. A. M. *J. Comput. Chem.* **2006**, *27*, 1009−1019.

(23) (a) Klamt, A.; Schuurmann, G. *J. Chem. Soc., Perkin Trans. 2* **1993**, 799−805. (b) Klamt, A. *J. Phys. Chem.* **1995**, *99*, 2224−4435. (c) Klamt, A.; Jonas, V. *J. Chem. Phys.* **1996**, *105*, 9972−9981. (d) Sinnecker, S.; Rajendran, A.; Klamt, A.; Diedenhofen, M.; Neese, F. *J. Phys. Chem. A* **2006**, *110*, 2235−2245.

(24) Boys, S. F.; Bernardi, F. *Mol. Phys.* **1970**, *19*, 553−566.

DOI: 10.1021/acs.organomet.5b00713
Organometallics XXXX, XXX, XXX−XXX